Rheol Acta 35:252–264 (1996)


ORIGINAL CONTRIBUTION

Ronald G. Larson
Suresh Goyal
Charles Aloisio

# A predictive model for impact response of viscoelastic polymers in drop tests

Received: 22 September 1995
Accepted: 19 January 1996

Dr. R.G. Larson (✉) · S. Goyal
Bell Laboratories, Lucent Technologies
700 Mountain Avenue
Murray Hill, New Jersey 017974, USA

C. Aloisio
2000 Northeast Expressway
Norcross, Georgia 30071-2903, USA

**Abstract** We show for the first time that a classical Hookean viscoelastic constitutive law for rubbery materials can predict the impact forces and deflections measured with a commercial drop tester when a mass, or "tup" with a flat impacting surface is dropped onto a flat pad of commercial impact-absorbing rubber. The viscoelastic properties of the rubber, namely the relaxation times and strengths, are obtained by a standard rheological linear-oscillatory test, and the equation of momentum transfer is then solved, using these measured parameters, assuming a uniaxial deflection of the pad during the impact. Good agreement between measured and predicted forces and deflections is obtained for a series of various drop heights, tup masses, impact areas, and pad thicknesses, as long as the deflection of the pad relative to its thickness is small or modest ($<50\%$ or so), and as long as the area of the pad is less than or equal to that of the tup. When the pad area is greater than the tup, forces are higher than predicted, unless an empirical factor is introduced to account for the nonuniaxial stretching of the ring of material that extends outside of the impact area. These results imply that the impact-absorbing properties of a rubbery polymeric material can be assessed by simply examining the material's linear viscoelastic spectrum.

**Key words** Constitutive equations – drop test – impact – linear viscoelasticity

## Introduction

Delicate devices are often protected against accidental impact by adding to them layers of rubbery shock-absorbing polymer; the optimal design of such layers can be achieved only if impact forces can be accurately predicted. Chen and Lakes (1990) have recently performed an analysis of impactors striking flat surfaces, and concluded that the ideal shock absorbing material has a loss tangent near unity for flat impactors, while a much higher loss tangent, of order 10, is best for spherical impactors. These predictions are helpful, but they strictly apply only to relatively small deflections, since they assume that the shock absorbing material is described by a linear viscoelastic constitutive equation.

For large uniaxial deformations, one can obtain a lower bound on the maximum force that will be produced by the impact by computing the constant force required to counteract the falling objects's kinetic energy within a distance equal to the thickness of the shock absorbing layer. One finds that a rubber pad of thickness "$x_0$" which must absorb the impact of a mass "$m$" moving with an impact velocity "$v_0$", generates a force "$F_m$" during the impact that reaches a value at least as high as $F_m = m v_0^2/2x_0$. However, this crude estimate assumes that the pad is compressed to zero thickness under the impact. Of course, under such large deformations, the

viscoelastic properties of the material will change greatly due to nonlinear effects, and the true impact stresses will be much larger than this estimate.

In the trade literature, semi-empirical procedures are proposed to account for the energy absorbed in realistic impacts. One such approach, described in more detail in Sect. 6, is the so-called "J curve", which is a plot of dimensionless impact force versus impact energy (Woolam, 1968). By measuring the J curve for a given material, deviations from ideal shock protection are quantified, and a basis for engineering design is provided. However, one can show (see section preceding conclusions) that the "J curve" is not a universal curve even for a single material, but varies with the conditions of impact.

Thus, as far as we know, no theoretical approach proposed so far accounts realistically for the forces generated during impacts that involve large, nonlinear deformations of the rubber layers. Also, the predictions of theories that do exist are rarely verified by comparison with experimental data. Here, therefore, we develop a simple impact model using a *nonlinear constitutive equation* for the rubber layer, namely that of the "rubber-like liquid" (Green and Tobolsky, 1946; Lodge, 1968). This viscoelastic model for rubbery *liquids* can be applied to rubbery *solids* merely by including long enough time constants in the material's relaxation spectrum. The constitutive equation is combined with Newton's third law for simple, uniaxial compressive impacts, and the predictions of the model are compared to measured forces during actual impact tests. We note that uniaxial impacts are equivalent to "equibiaxial deformations" whose study was pioneered by Joachim Meissner and coworkers (Meissner et al., 1982).

In the next section, we describe the factors that will in general affect the impact forces during a drop test. Then, in the following section, we describe our experimental procedure for measuring impact forces and deflections as well as the viscoelastic material properties needed by the simple model. The model is then described; next, the predictions of this model are compared to the experimental drop tests, then the validity of a traditional engineering design concept, "the J Curve," is explored. Results and future directions are summarized in the final section.

## Factors affecting impact

When a compliant material (e.g., an impact-absorbing rubber) is impacted between two rigid, colliding surfaces, there are several important factors that control the impact forces that are produced. First, there is the viscoelastic character of the impact-absorbing rubber – i.e., its frequency-dependent modulus or compliance – for both small and large deformations, that is, in the linear and nonlinear regimes of deformation. Second, there are the shape of the rubber and its shape changes during impact; these shape changes will in general be complex and nonlinear, influencing the forces produced. Third, there are the interfacial adhesive characteristics between the rubber and each of the hard impacting surfaces. Fourth, there is the volume change in the rubber as it undergoes impact; although any volume change will be small, it can be associated with large forces that are related to the material's bulk modulus. And fifth, there is the propagation of the viscoelastic shock wave that moves through the rubber immediately after impact.

### Viscoelasticity of the rubber

We will account for the viscoelasticity of the material using a simple constitutive equation for ideal rubber, to be presented later. This equation requires as inputs linear viscoelastic parameters, namely a spectrum of relaxation times and associated relaxation strengths or moduli, which can be extracted from the frequency-dependent storage and loss moduli also presented later.

### Shape and shape changes

The traditional way to account for the shape of the rubber pad and to normalize between impact forces from pads of different shapes is through a non-dimensional parameter, called the shape factor, $S$ (Freakley and Payne, 1978). It is defined to be the ratio of the surface area of the pad bearing the load to the unloaded, free surface area. The shape factor can be illustrated through the simple case of a round cylindrical disk undergoing uniaxial compression (Fig. 1 a). The loaded areas of the pad are the two circular surfaces that contact the tup and the substrate on which the pad rests; the unloaded area is around the perimeter of the pad. Hence for this case, the shape factor changes according to the following formula

$$S \equiv \frac{\text{loaded area}}{\text{unloaded area}} = \frac{2\pi D(t)^2/4}{\pi D(t)x(t)} = \frac{D(t)}{2x(t)} \tag{1}$$

Since the thickness $x(t)$ of the pad decreases during impact, and the diameter $D(t)$ increases, the shape factor increases continuously during the impact. More complex shape changes are also possible; when the area of the pad becomes larger than that of one of the impacting surfaces, the material outside of the area of impact will deform as shown in Fig. 1 b.

### Interfacial adhesion

The shape and deformation of the rubber during impact is affected by the adhesive characteristics of the interfaces

Rheologica Acta, Vol. 35, No. 3 (1996)


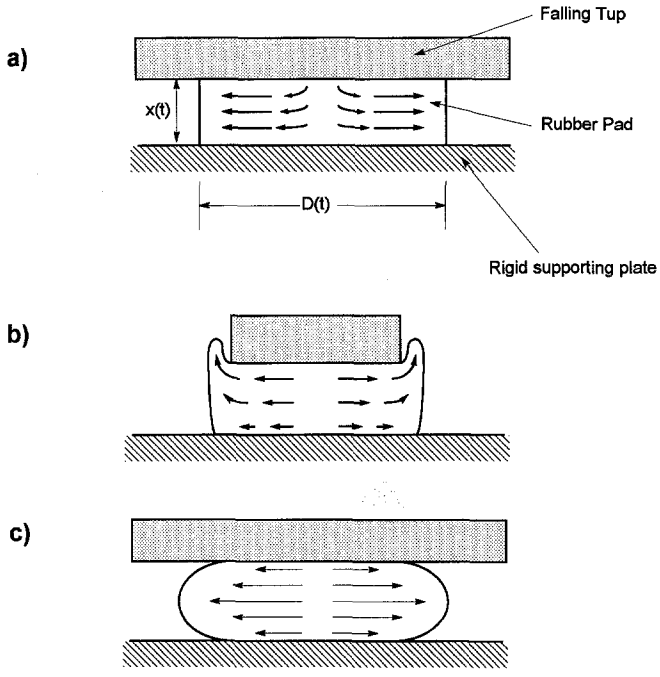


**Fig. 1** Possible modes of deformation of a cylindrical rubber pad during impact between two hard flat surfaces. a) Perfect slip with pad diameter smaller than the hard surfaces, producing a simple uniaxial deformation; b) pad diameter becomes larger than that of the tup, leading to nonuniform deformation such as bulging at the edges; c) adhesion between the rubber pad and the hard surfaces, producing a shearing deformation, combined with uniaxial deformation

between the rubber and the hard surfaces. For the case of ideal slip, depicted in Fig. 1 a, the rubber changes shape uniaxially. But if the rubber adheres strongly to the hard surfaces, then elements of rubber that are next to these surfaces cannot slide, and the rubber will experience shearing deformations, combined with uniaxial compression (see Fig. 1 c).

## Volume changes

For a very large shape factor, that is for a thin, wide pad, even small changes in pad thickness during impact involve large deformations of material. This configuration has been studied extensively in tension because of the unusual failure mode of soft rubbers under these constraints (Gent and Lindley, 1959). In the case of impact described here with large $S$ the material may reduce the amount of lateral deformation required by shrinking its volume somewhat. That is, the impact may produce bulk compression, which is governed by the material's bulk *compressive modulus* $K$, which is related to the tensile modulus "$E$" and Poisson's ratio "$\nu$" as $K = \frac{E}{3(1-2\nu)}$.

Due to the frequency dependence of $\nu$, the bulk modulus $K$ may be a different function of frequency than are the tensile and shear moduli discussed in the next section. A diameter-to-thickness ratio greater than 3–4 is typically high enough to produce near-hydrostatic tension in the center of the sample (Gent and Lindley, 1959; Lindsey et al., 1963). This range of diameter-to-thickness ratios corresponds to a shape factor $S$ in the range 1.5–2.0.

## Viscoelastic shock waves

Finally, for hard impacts, viscoelastic shock waves may be launched into the rubbery material. Such waves travel at a characteristic wave speed given by $\sqrt{G/\varrho}$, where $G$ is a characteristic modulus, roughly $10^8$ dyn/cm$^2$, and $\varrho$ is the material's density, roughly 1 gm/cm$^3$. Thus the wave speed is around $10^4$ cm/s, and will traverse the thickness of a 1 cm thick pad in around 0.1 ms. Because the shock-absorbing material is dissipative ($G''$ is not zero), the wave will disperse as it travels, and eventually the deformation will distribute itself uniformly throughout the thickness of the layer. Unless the impact is unusually violent, the material has a low modulus, or the pad is especially thin, we expect that the shock wave will disappear in a time short in comparison to the duration of the impact (typically around 1 ms), and can therefore be ignored.

Our goal is to understand the role that such factors play in impacts typical of those encountered by consumer products in everyday environments. To accomplish this, each factor must be isolated as much as possible from the others. Here, we concentrate on the first factor, the viscoelasticity of the rubber; thus our experiments are carried out under conditions that minimize the role of the other factors. As a starting point, we will here consider the case of a hard cylindrical tup having a flat surface (see the next section), which impacts against the flat face of a cylindrical rubber "pad" whose area of impact is smaller than that of the tup, so that the rubber pad does not extend beyond the tup during the impact. If the rubber surface slips against that of the tup, the deformation is then expected to be a simple uniaxial deformation, similar to that depicted in Fig. 1 a. In addition, we keep the thickness of the pad moderate or high, so that the shape factor remains small enough that bulk compression does not become a significant factor. Finally, the impact velocities are small to modest, so that the deformation of the rubber is not too severe. We will show that, under the above conditions, the impact is governed by the frequency-dependent shear modulus of the rubber; and a simple theory, discussed in the fourth section, should, in principle, describe the impact.

## Experimental

### Material

All experiments described in this paper were done using 70 durometer Sorbothane rubber, supplied by Sorbothane Incorporated of Kent, OH. Sorbothane is a popular shock-absorbing material because of its highly dissipative character, its wide temperature performance range, and its low cost. It is reported to be a two-part polyether polyurethane. The starting polyol is combined with an isocyanate from BASF (most likely aliphatic) in a greater than 8/1 ratio. The 70 durometer material used in this study has a rubbery tensile modulus of 120 psi. A 65 durometer Sorbothane tested earlier had a rubbery tensile modulus of 70 psi. These materials are lightly crosslinked polymers.

### Viscoelastic measurements

The viscoelastic properties of the 70 durometer Sorbothane rubber used in the tests reported on here were characterized by small-amplitude oscillatory tests using the Rheometrics Solids Analyzer in tension-tension mode. The sample was 22.88 mm long, 3.96 mm wide, and 1.04 mm thick. The applied strain amplitude varied from a low of 0.03% at −80 °C to a high of 0.1% at 80 °C. At the lowest temperature, a static tensile stress of 86 psi (around 0.6 MPa) was applied and at the highest temperature this was reduced to almost zero.

At each of the temperatures in Table 1, the tensile storage modulus $E'$ and the tensile loss modulus $E''$ were measured at frequencies ranging from 0.1 to 100 radians/s. Because of the equivalent effect of frequency and temperature (Lindsey et al., 1963; Ferry, 1980), in the absence of any structural or chemical changes during the test, the moduli at each individual temperature can be shifted along the log frequency axis to form a master curve at the reference temperature of 20 °C. The shift factors for each temperature are tabulated in Table 1; the master curve appears in Fig. 2.

**Table 1** Viscoelastic shift factors for Sorbothane 70

| Temperature (°C) | $\log_{10} a_T$ |
|---|---|
| −81 | 13.87 |
| −70 | 13.27 |
| −61 | 10.97 |
| −50 | 8.67 |
| −40 | 6.37 |
| −30 | 4.53 |
| −20 | 3.23 |
| −10 | 2.19 |
| 0 | 1.39 |
| 9 | 0.6 |
| 19 | 0 |
| 29 | −0.2 |
| 39 | −0.6 |
| 50 | −0.8 |
| 59 | −1.0 |
| 80 | −2.2 |

The shear storage and loss moduli, $G'$ and $G''$, are related to the corresponding tensile moduli by

$$G' = \frac{E'}{2(1+\nu)} \; ; \quad G'' = \frac{E''}{2(1+\nu)} \tag{2}$$

In the low-frequency, low-modulus rubbery zone, Poisson's ratio $\nu \approx 0.5$, and Eq. (2) reduces to $G' = E'/3$, and

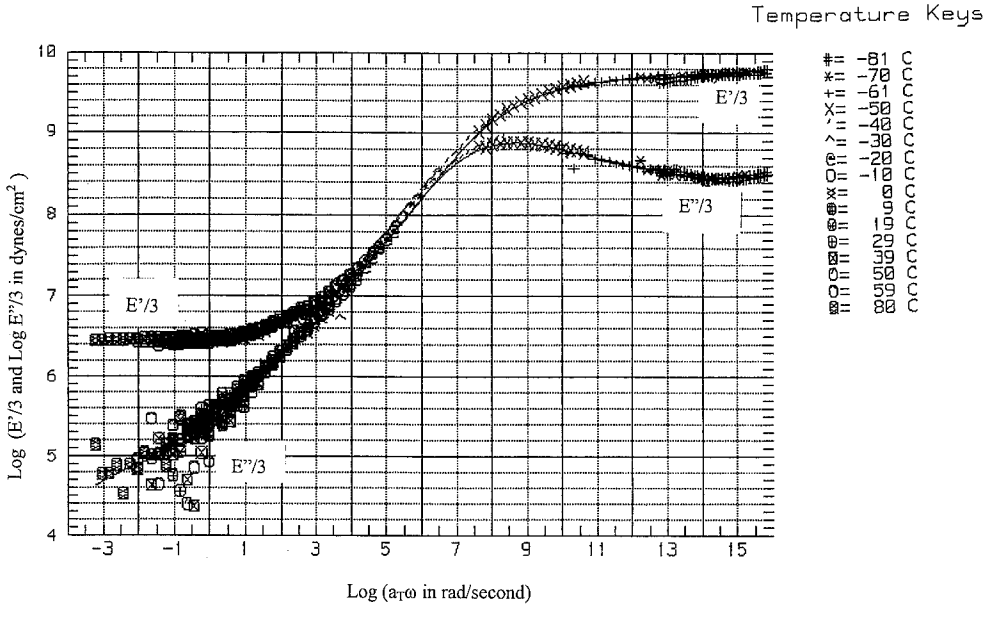


**Fig. 2** "Master Curve" of $E'/3$ and $E''/3$ versus reduced frequency $\log(a_T\omega)$ for Sorbothane 70, produced by sliding curves obtained at each temperature listed in the temperature keys along the log frequency axis by an amount $\log a_T$, given in Table 1, to obtain a superposition at a reference temperature of 20 °C

$G'' = E''/3$. These relationships are used for all of the data in Fig. 2. Although in the high-frequency, high-modulus, glassy zone, Poisson's ratio is actually less than 0.5, the data in this region are not important to the impact properties of the material, as we will discuss below.

The shift factors $\log a_T$, obtained during the construction of the master curve, are plotted versus temperature in Fig. 3. The temperature keys in Fig. 2 aid in seeing where specific temperatures contribute to the master curve where the data point density is not too great. Once a spline fit for the master curve is obtained, transient functions such as creep and stress relaxation are readily calculated at various temperatures using the $\log a_T$ data.

Using a so-called "WLF fit" to the data of Fig. 3 (see Ferry, 1980), a glass transition temperature of approximately $-60\,^{\circ}C$ was determined, and the thermal expansion coefficient for the free volume was estimated to be $3.249\times10^{-4}$, in good agreement with literature values (Ferry, 1980). The constants for the glass transition reference are $c_1^g = 17.44$ (assigned) and $c_2^g = 76.64$ (calculated).

The ratio of $E''$ to $E'$, called $\tan\delta$, is a useful measure of the damping characteristics of viscoelastic materials. The knowledge of the form of the master curve, and use of the shift factors can aid in designing materials for specific ranges of frequency and temperature performance. Figure 4 shows the tensile storage modulus $E'$ and

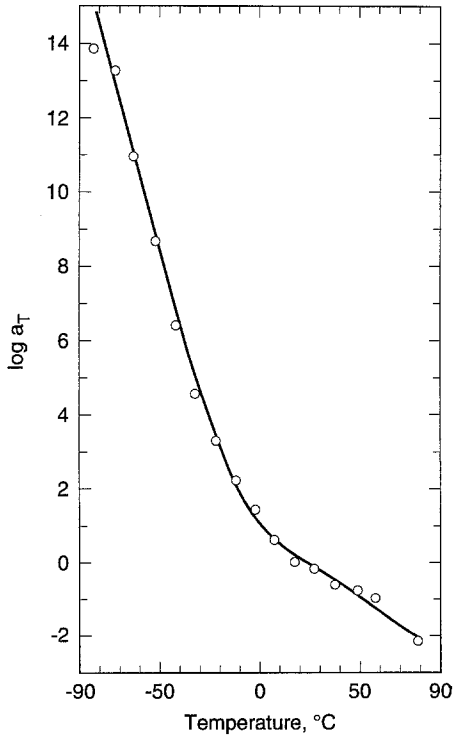


**Fig. 3** Plot of the shift factors used to obtain the master curve of Fig. 2, versus temperature

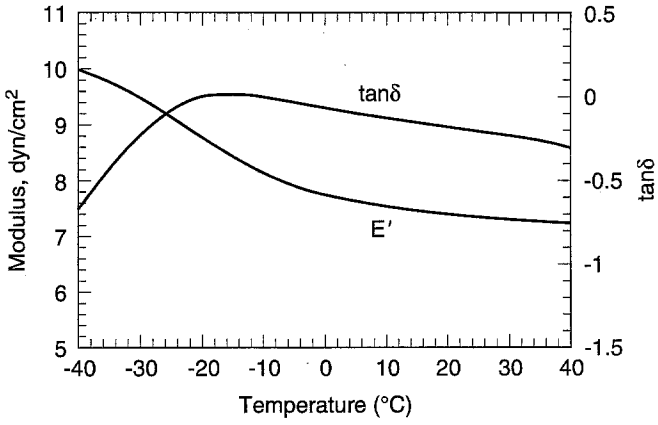


**Fig. 4** The temperature dependence of the tensile storage modulus $E'$ and the loss tangent $\tan\delta$ for Sorbothane 70 at a frequency of 1000 radians/s, computed from the master curve, Fig. 2

$\tan\delta$ for a frequency of 1000 radians/s. As will be discussed in what follows, the frequency of 1000 radians/s is roughly in the center of the window of impact sensitivity in our experiments. Note the broad peak in $\tan\delta$ at around $-15\,^{\circ}C$; this peak shifts to $-23\,^{\circ}C$ when the frequency is reduced to 100 radians/s. The shape of the $\tan\delta$ curve and its shift with temperature or frequency are considered to be important to the impact properties of this material. Specifically, the existence of a peak in $\tan\delta$ at $-15\,^{\circ}C$ at the frequency of 1000 radians/s implies that under typical impact conditions the material will be the most dissipative at this temperature, and hence at this temperature will most readily dissipate the mechanical energy of impact into heat. Thus the rebound velocity after dropping a device protected by such a material would be a minimum at this temperature, other factors being held fixed. In the following section, we show by drop testing that, indeed, the mechanical energy dissipation in this material increases as the temperature is reduced below room temperature.

## Drop tests

Drop-test data for the Sorbothane rubber pads were collected using Dynatup impact testing machine Model 8250, shown schematically in Fig. 5. The main element of the machine is a variable mass, called the crossheat, that can be dropped from a given height onto the rubber pad being tested. High impact velocities can be obtained by propelling the crosshead with springs. (This feature was not needed in the experiments reported here.) The crosshead is guided on frictionless vertical rails to control its orientation. The impact force is measured through a load cell mounted on the element of the crosshead that first makes contact, which is the tup. Different inserts can be screwed to the tup to change contact geometry. The

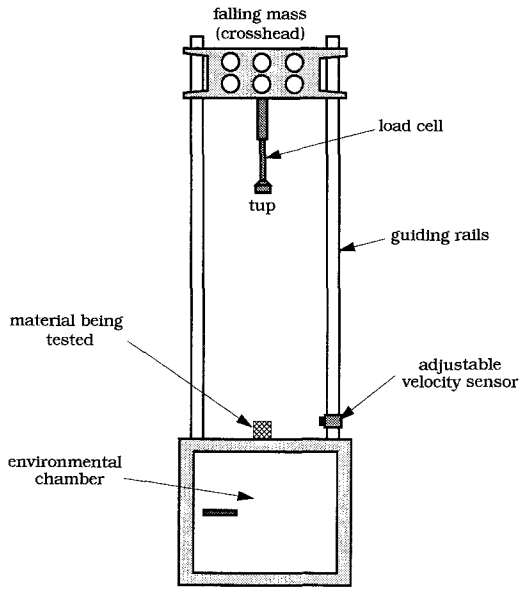


**Fig. 5** Schematic of Dynatup impact testing machine Model 8250 used to test the impact response of rubber pads. The machine allows a known mass (the crosshead) to be dropped from a given height onto the material being tested. Drop orientation is controlled through frictionless guiding rails. An optical sensor measures impact velocity and a load cell measures force. The environmental chamber can be used to test materials at temperatures other than room temperature

specimen temperature can be controlled in an environmental chamber. An automated data acquisition system collects and analyzes the data. The acceleration can be obtained from the force by dividing by the mass of the crosshead. Besides the initial impact velocity (measured independently through an optical sensor), other parameters, such as pad deflection, can be calculated from the acceleration by integration.

We used cylindrical tup inserts made of Aluminium 7075 with flat contacting areas, varying in diameter from an inch to 2.5 inches (2.54 to 6.35 cm), rubber pads ranging from disks an inch (2.54 cm) in diameter to squares 6 inches (15.24 cm) on a side, with thicknesses ranging from 0.5 to 2.0 inches (1.27 to 5.08 cm); and crosshead masses from 3.99 to 26.83 lbs (1.81 to 12.18 kg). The flat supporting plate was made of 316 Stainless Steel with a blanchered ground finish to ensure flatness. Impact data were collected at room temperature, which was 20 °C, and at −5 °C and 40 °C.

## Impact model

For a simple uniaxial impact, Newton's second law gives a relationship between the impact force $F = m\ddot{x}$ and the uniaxial stress $\sigma$ in the material:

$$m\ddot{x}(t) = A(t)\sigma(t) \ , \tag{3}$$

where $m$ is the mass of the tup (really of the tup and the entire crosshead assembly), $A(t)$ is the instantaneous area of impact, and $\ddot{x}(t)$ is the instantaneous acceleration. When the area of impact of the tup is greater than that of the pad throughout the impact, the area $A(t)$ is inversely proportional to the instantaneous thickness of the pad; i.e.,

$$A(t) = \frac{A_0 x_0}{x(t)} \ , \tag{4}$$

where $A_0$ is the initial area of the pad.

We propose that the instantaneous viscoelastic uniaxial stress $\sigma = \sigma_{ve}$ can be obtained from a model constitutive equation for an ideal Hookean incompressible viscoelastic material (Green and Tobolsky, 1946; Lodge, 1964; Treloar, 1975):

$$\sigma_{ve} = \int_{-\infty}^{t} m(t-t')[\lambda(t,t') - \lambda^{-2}(t,t')]\,dt' \ . \tag{5}$$

Here, $\lambda(t,t')$ is the deformation produced during the time interval between time $t'$ and time $t$; it is defined as $\lambda(t,t') \equiv x(t')/x(t)$. The above formula assumes that the deformation is a purely uniaxial one, which implies that the rubber does not adhere strongly to the surface of the tup, which, as discussed earlier, would lead to shearing deformations.

The function $m(t-t')$ contains the material's viscoelastic properties; this function is derived from the time-dependent linear modulus $G(t-t')$ using

$$\frac{dG(t-t'}{dt')} \equiv m(t-t') \tag{6}$$

The linear modulus $G(t-t')$, in turn, can be extracted from the dynamic oscillatory data for Sorbothane 70 presented earlier. It is convenient to represent $G(t-t')$ by an analytic form, a sum of exponentials:

$$G(t-t') = \sum_i G_i e^{-(t-t')/\tau_i} \ , \tag{7}$$

where $\tau_i$ and $G_i$ are the relaxation times and strengths obtained by fits to the $G'$ and $G''$ data for Sorbothane. The frequency-dependent moduli $G'(\omega)$ and $G''(\omega)$ are related to the $\tau_i$'s and $G_i$'s by

$$G'(\omega) = \sum_i \frac{G_i \omega^2 \tau_i^2}{1+\omega^2\tau_i^2} \ ; \quad G''(\omega) = \sum_i \frac{G_i \omega \tau_i}{1+\omega^2\tau_i^2} \tag{8}$$

Now, we choose a set of $\tau_i$'s with a reasonably dense spacing in the log time domain, and adjust the values of

the corresponding $G_i$'s to obtain a "best fit" between Eq. (8) and the experimental $G'$, $G''$ data. Figure 6 shows that a good fit over the frequency range $10^{-2}-10^4$ rad/s is obtained this way using a 14- or 15-mode fit, with the constants given in Table 2. The fit to the $G'$ and $G''$ values predicted using the first 14 modes fails for frequencies higher than $10^4$ rad/s, while for 15 modes, the fit can be extended out to around $10^5$ rad/s. The frequency above which a fit is no longer obtainable is set by the reciprocal of the shortest relaxation time $\tau_i$ in the assumed spectrum. From Table 2, this shortest time constant is $10^{-4}$ s for the 14-mode fit, and is $10^{-5}$ s for the 15-mode fit. Hence fits at frequencies higher than $10^5$ are not possible unless the spectrum is extended to include still shorter relaxation times. However, it is unnecessary to include modes with time constants that are very much shorter than the duration of the impact, which is several ms, because these modes contribute little to the material's viscoelastic response under impact. Such very fast modes are almost completely relaxed on the time scale of the impact, and contribute only a small viscous-like dissipative stress.

The dissipative stress due to fast modes can, if desired, be accounted for in the impact model by adding a small viscous term to the unaxial stress:

$$\sigma = \sigma_{ve} + 3\eta\dot{\lambda}(t) \ , \tag{9}$$

where $\eta$ is the viscosity associated with the fast modes. $\eta$ is obtained by choosing its value to be that which permits the fit to $G''$ to be extended out to a frequency of $10^5\ s^{-1}$ for the 14-mode spectrum, and to $10^6\ s^{-1}$ for the 15-mode one. For the 14-mode spectrum, this gives

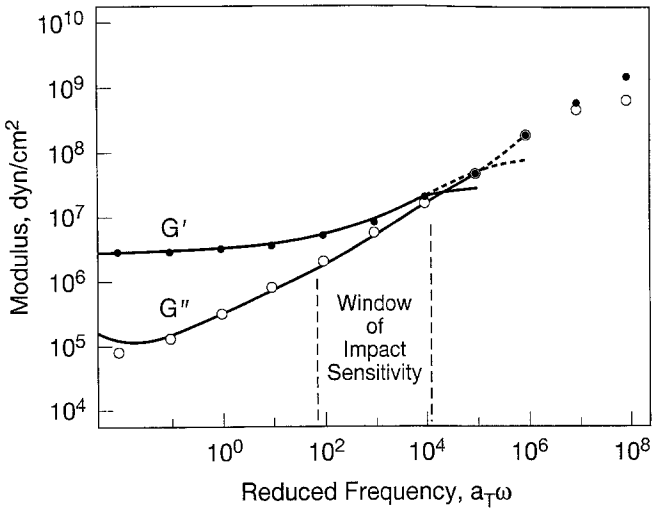


**Fig. 6** Prediction of $G'$ and $G''$ using the 14-mode spectrum plus a viscous term with a viscosity of 500 Poise (solid lines) and the 15-mode model with a viscosity of 200 Poise (dotted line), compared to the linear viscoelastic data for Sorbothane 70, shifted to 20 °C

**Table 2** Viscoelastic constants for Sorbothane 70 at 20 °C

| $i$ | $\tau_i$ (s) | $G_i$ (dyn/cm²) |
|---|---|---|
| 1 | 10000 | 0.27e+07 |
| 2 | 1000 | 0.004e+07 |
| 3 | 100 | 0.007e+07 |
| 4 | 30 | 0.008e+07 |
| 5 | 10 | 0.009e+07 |
| 6 | 3 | 0.010e+07 |
| 7 | 1 | 0.020e+07 |
| 8 | 0.3 | 0.030e+07 |
| 9 | 0.1 | 0.05e+07 |
| 10 | 0.03 | 0.05e+07 |
| 11 | 0.01 | 0.1e+07 |
| 12 | 0.003 | 0.2e+07 |
| 13 | 0.001 | 0.3e+07 |
| 14 | 0.0001 | 1.9e+07 |
| 15 | 0.00001 | 5.0e+07 |

$\eta = 500$ Poise. For 15-modes, the best-fit value, $\eta = 200$, is smaller than that for 14 modes because for the former more of the high frequency relaxation processes are included explicitly in the discrete spectrum.

The adequacy of this representation of the viscoelastic spectrum for our purposes was tested by integrating Eq. (3) both with the 14-mode spectrum with $\eta = 500$ Poise, and with the 15-mode one with $\eta = 200$ Poise. Almost identical results are obtained in the two cases, proving that the 14-mode spectrum is adequate.

The explicit inclusion of very fast modes is to be avoided, because it would unnecessarily slow the numerical integration of Eq. (3); the time step of the explicit integration of Eq. (3) must be smaller than the smallest relaxation time in the spectrum so that numerical stability is preserved.

While modes much faster than the characteristic impact frequency can be lumped into a viscous term, modes much slower than this frequency could be lumped into a purely elastic term, with an infinite relaxation time. The portion of the relaxation frequency spectrum to which we expect the impact to be sensitive in our tests is indicated in Fig. 6; the material response outside of this frequency window could probably be represented by a combination of a purely elastic and a purely viscous response. However, inclusion of slowly relaxing modes, unlike the fast relaxing ones, does not force a reduction of the integration time step size, and so is not numerically expensive. Therefore, we shall here include the slow modes of Table 2 explicitly, and not lump them into an effective elastic term.

When the deformation of the rubber exceeds about 15% or so, nonlinear viscoelastic effects come into play. These are represented in Eq. (5) by the nonlinear dependence on $\lambda$, which is taken from rubber elasticity theory (Treloar, 1975). This theory assumes that the elasticity of the polymer chains obeys Hooke's law. This is equivalent to the requirement that a network chain's equilibrium dis-

tribution of lengths, under the effects of thermal fluctuations, obey Gaussian statistics. This assumption can be expected to break down for severe deformations. The deformations for which non-Hookean or non-Gaussian effects occur depend on the rubber's cross-link density; the higher the cross-link density, the smaller the deformation at which non-Gaussian effects will occur.

## Comparison of theory and experiment

With the viscoelastic properties of the Sorbothane 70 rubber characterized as described earlier, we can now predict the forces generated during impact by solving Eq. (3), *with no adjustable parameters*. For a given material at a fixed temperature, four experimental impact parameters can readily be varied: the velocity of impact, the mass of the impacting tup, the thickness of the pad, and the diameter of the pad. In principle, the effects of all these parameters on the curve of impact force versus time or deflection should be predicted by the simple theory. The temperature can also be varied to see if the impact force changes as predicted by the theory using the viscoelastic shift factors. Finally, the area of the pad can be made larger than that of the tup, so that sample bulges out from under the tup during the impact. In this way, we can examine experimentally the effect of irregular deformation, illustrated in Fig. 1 b. We also briefly discuss materials other than Sorbothane 70.

### Varying impact velocity

Figure 7 shows the curves of force versus deflection measured for a pad of Sorbothane 70, 2.49 cm in diameter and 2.54 cm thick, impacted by a 3.81 cm diameter tup of mass 1.81 kg, at velocities ranging from 1.0 to 2.84 m/s. Note that the force begins its pronounced rise at a deflection somewhat greater than zero (around 0.05 cm). This offset from zero deflection is believed to be caused by premature triggering of data collection by the computer during the impact. In the theory, we correct for it by simply shifting the theoretical predictions by the offset amount, which is readily estimated from plots such as Fig. 7. In Fig. 7 (and all other figures), the plotted symbols are experimental data points, and the lines are the predictions of Eq. (3), using the 14-mode fit to the linear relaxation data, shown in Table 2. One of the calculations, the one for the highest impact velocity, was re-done with the 15-mode spectrum; the result is almost identical to that for the 14-mode spectrum, as shown. Even closer agreement between the 14- and 15-mode spectra is obtained for lower impact velocities. This shows that a 14-mode representation of the linear viscoelastic data is adequate for these experiments.

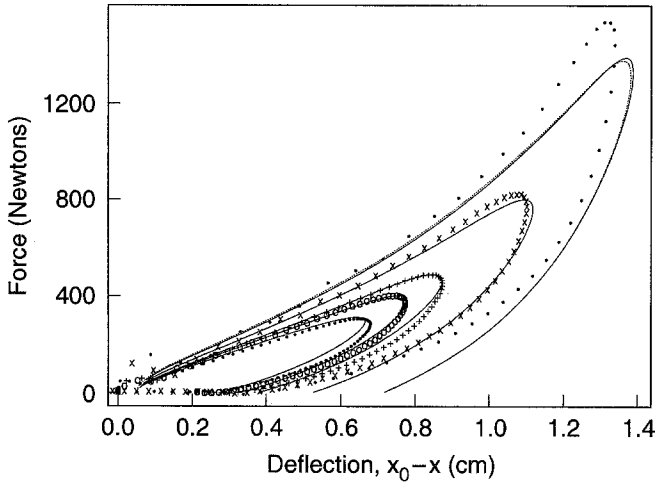


**Fig. 7** Curves of force against sample deflection, for a sample of Sorbothane 70, with initial diameter $D_0 = 2.49$ cm, and thickness $x_0 = 2.54$ cm, impacted by a tup of diameter 3.81 cm and mass 1.81 kg at velocities of $v_0 = 1.0$, 1.23, 1.44, 2.04, and 2.84 m/s, at $T = 20 \pm 1$ °C. The lines are the predictions of Eq. (3), with an offset deflection of 0.05 cm. For the velocity of 2.84 m/s, there are two lines; one is for the 14-mode fit representation of the linear viscoelastic data with $\eta = 500$ Poise, and the other is for the 15-mode representation with $\eta = 200$ Poise. All other calculations were made with the 14-mode spectrum

The agreement between theory and experiment in Fig. 7, with no adjustable parameters (except for the offset deflection), is very good, at least for impact velocities less than or equal to 2 m/s. For the highest impact velocity, 2.84 m/s, the pad is deflected by over 1.27 cm, which is 50% of the original pad thickness. Under these conditions, the maximum impact force is around 10% higher than predicted, perhaps because of the non-Gaussian effects discussed earlier, or because of shearing contributions to the deformation due to adhesion of the rubber to the tup or substrate.

### Varying mass

An analogous family of curves is generated when one varies the mass of the tup, holding the impact velocity roughly constant at about 1.0 m/s (see Fig. 8). Again, for the hardest impact, with a tup mass of 12.18 kg, pad deflections of greater than 50% are seen, and the theory begins to fail.

### Varying pad thickness

Figure 9 a – c shows the changes in the families of curves for various impact velocities that occur for pads of thicknesses 1.37, 2.69, and 3.71 cm, all of diameter 3.78 cm. As the pad thickness increases, the forces generated by the

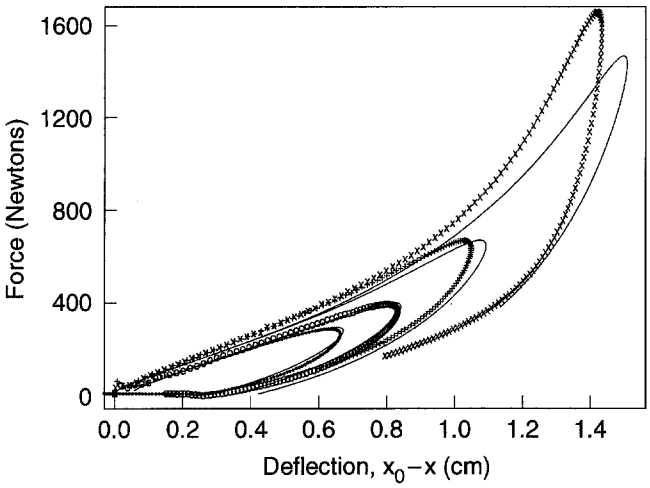


**Fig. 8** Curves of force against sample deflection, for a sample of Sorbothane 70, with initial diameter $D_0 = 2.49$ cm, and thickness $x_0 = 2.54$ cm, impacted by tups of diameter 3.81 cm and masses of 1.83, 2.71, 5.33, and 12.18 kg, at $T = 20 \pm 1$ °C. The velocities of these four masses were all roughly equal, namely 1.01, 1.07, 1.06, and 1.05 m/s, respectively. The lines are the predictions of Eq. (3), with an offset deflection of 0.05 cm for the two smaller masses, and 0.0 cm for the larger two masses

impact decrease, as predicted by Eq. (3). Note that for the thickest pad, the forces are somewhat less than predicted by the theory. For an even thicker pad, 5.08 cm, these deviations become even greater. We suspect that these very thick pads *buckle slightly* during the impact, which leads to a greater-than-predicted deformation, and a lower force.

## Varying temperature

We can also consider the effect of temperature on the impact forces, by using the shift factors $a_T$, given in Table 1. These were obtained by the time-temperature superposition used to obtain the master curve plotted in Fig. 2. These shift factors allow us to predict impact stresses at temperatures other than 20 °C simply by multiplying all relaxation times in Table 2 by $a_T(T)$ to account for changes in temperature. Here we consider just two other temperatures: a "low" temperature, −5 °C, and a "high" temperature, 40 °C. From Table 1, we estimate $a_T = 69$ at −5 °C, and $a_T = 0.25$ at 40 °C. To predict the impact forces at −5 °C, we multiply each relaxation time in the 15-mode spectrum, as well as the viscosity $\eta = 200$ Poise, by a factor of 69. For $T = 40$ °C, we multiply each relaxation time in the 14-mode spectrum, and the viscosity $\eta = 500$ Poise, by a factor of 0.25. We use the 15-mode spectrum at the low temperature, because at low temperature the shift factor greatly exceeds unity and all the relaxation times become much larger than at 20 °C; thus the shortest relaxation time in the 14-mode spectrum is

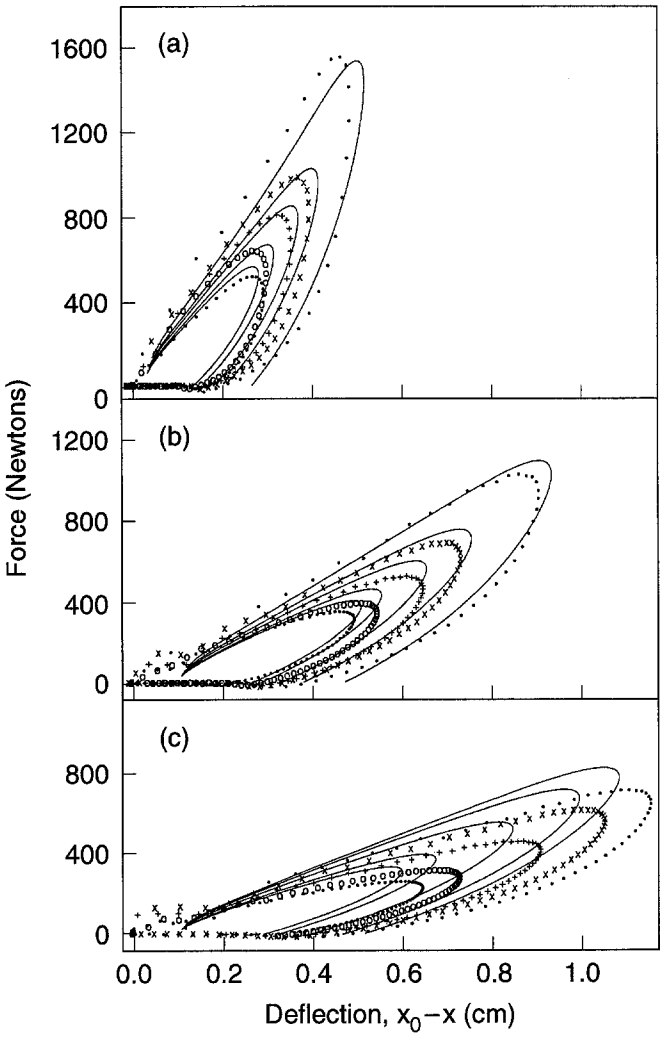


**Fig. 9** Curves of force against sample deflection, for a sample of Sorbothane 70, with initial diameter $D_0 = 3.78$ cm, and thicknesses of a) 1.37 cm, b) 2.69 cm, and c) 3.71 cm, impacted by a tup of diameter 5.08 cm and mass 1.83 kg, at $T = 20 \pm 1$ °C. In a) the velocities are 0.97, 1.12, 1.38, 1.60, and 2.14 m/s; in b) the velocities are 1.02, 1.15, 1.44, 1.74, and 2.33 m/s; and in c) the velocities are 1.01, 1.19, 1.59, 1.97, and 2.21 m/s. The lines are the predictions of Eq. (3), with an offset deflection of a) 0.025, b) 0.10, and c) 0.10 cm

0.0069 at −5 °C. A shorter time constant than this is needed to be sure that the relaxation processes are adequately represented in the frequency window $10^2 - 10^4$. (We also tried a 16-mode spectrum for simulations at $T = -5$ °C containing a 10-fold shorter relaxation time than is contained by the 15-mode spectrum, but the results for the 15- and 16-mode spectra differed very little from each other, so the 15-mode spectrum was deemed adequate for the low-temperature experiments.)

In Fig. 10a–b, the impact forces versus deflection are plotted for impacts at −5 °C and 40 °C for the same 2.49 cm diameter pad used to obtain the data at room temperatures plotted in Fig. 7. At the low temperature, the

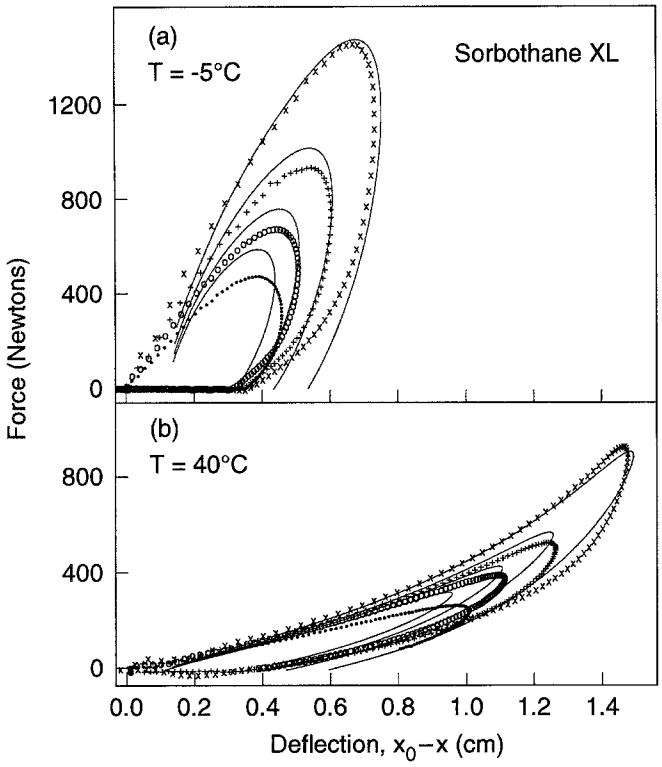


**Fig. 10** Curves of force against sample deflection, for a sample of Sorbothane 70, with initial diameter $D_0 = 2.49$ cm, and thickness of 2.59 cm, impacted by a tup of diameter 3.81 cm and mass 2.57 kg, at a) $T = -5 \pm 1\,°C$, and b) $40 \pm 1\,°C$. The impact velocities are a) 1.00, 1.26, 1.64, and 2.22 m/s, and b) 0.96, 1.20, 1.46, and 1.95 m/s. The lines are the predictions of Eq. (3), with offset deflections of a) 0.10, and b) 0.12 cm

impact forces are larger and the deflection less than at high temperature. This is an obvious consequence of the increased stiffness of the material at low temperature. Note also that the hysteresis is less at high temperature than at low temperature, evidently caused by the increased elastic character of the material at high temperature. Note in Fig. 6 that the storage modulus $G'$ becomes increasingly greater than the loss modulus $G''$ as the frequency decreases. As the temperature increases, the low-frequency, less lossy behavior is shifted into the frequency range $10^2 - 10^4$ that most affects impact: the result is a more elastic response. At low temperature, the hysteresis is high, indicating a high conversion of mechanical energy into heat, presumably because there is a peak in the loss tangent near $T = -15\,°C$ at the characteristic impact frequency of around 1000 radians/s (see Fig. 4 and the discussion in the third section). Thus the level of "deadness" of the rubber, measured by the size of the hysteresis loop, is maximized at a temperature considerably below room temperature.

Note in Fig. 10 that these changes in impact performance with temperature are faithfully captured by the theory. However, for unknown reasons, the behavior at small impact velocities is modeled less successfully at depressed and elevated temperatures than was the case at room temperature (compare Figs. 7 and 10).

Apart from the deviations sometimes observed at either the highest or lowest impact velocities, and the deviations observed for very thick pads, there is generally excellent qualitative and even quantitative agreement between theory and experiment, not only in the maximum force, but also in the shape of the hysteresis when the material rebounds. This proves that, under these conditions, the impact is governed almost entirely by the viscoelastic properties of the rubber in a simple uniaxial deformation. Thus the effects of shape factor, interfacial adhesion, or volume changes are not major factors under the conditions of impact studied so far.

As a pad is squeezed during impact, its area increases, producing larger forces and smaller deflections than one would obtain if the area of impact were held constant. Figure 11 shows the force versus deflection curves that we compute by arbitrarily holding the impact area constant at its initial value, compared to the curves one generates by allowing the impact area to increase according to Eq. (4). Clearly the growth in impact area during impact greatly increases the maximum impact force for high impact velocities.

## Varying pad size with fixed tup diameter

Next, we test the predictions of the theory for constant impact area by using pads that are larger than the area of the tup, so that the impacted area under the tup is constant during the impact. Figure 12 shows impact force vs.

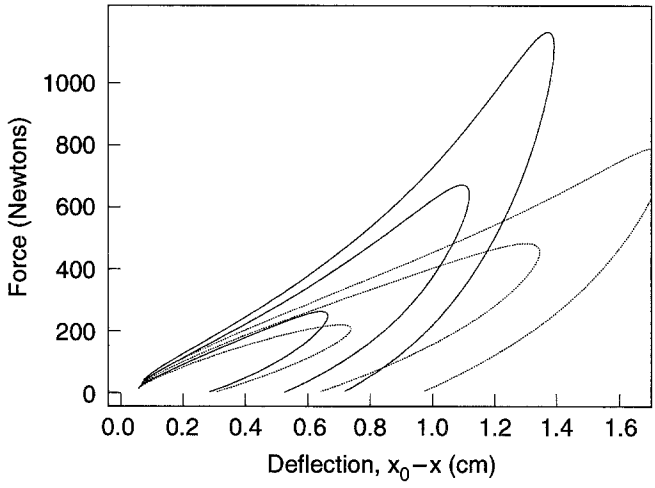


**Fig. 11** The solid lines are the theoretical lines from Fig. 7 with impact velocities $v_0 = 1.00$, 2.04, and 2.84 m/s, while the dashed lines were obtained from the theory under the same conditions as the solid lines, except the impact area was held fixed at its initial value throughout the impact

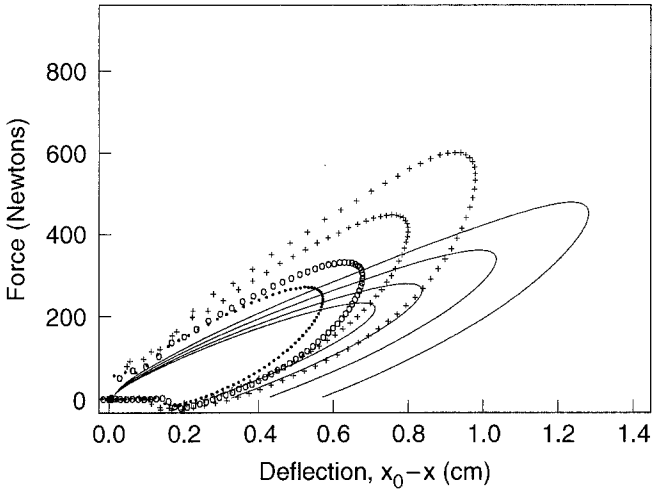


**Fig. 12** Curves of force against sample deflection, for a sample of Sorbothane 70, with initial diameter $D_0 = 3.78$ cm, and thickness 2.69 cm, impacted by a tup of diameter 2.54 cm and mass 1.79 kg, at $T = 20 \pm 1$ °C. The impact velocities are 1.01, 1.22, 1.55, and 1.98 m/s. The lines are the predictions of Eq. (3) with a constant impact diameter equal to that of the tup, 2.54 cm

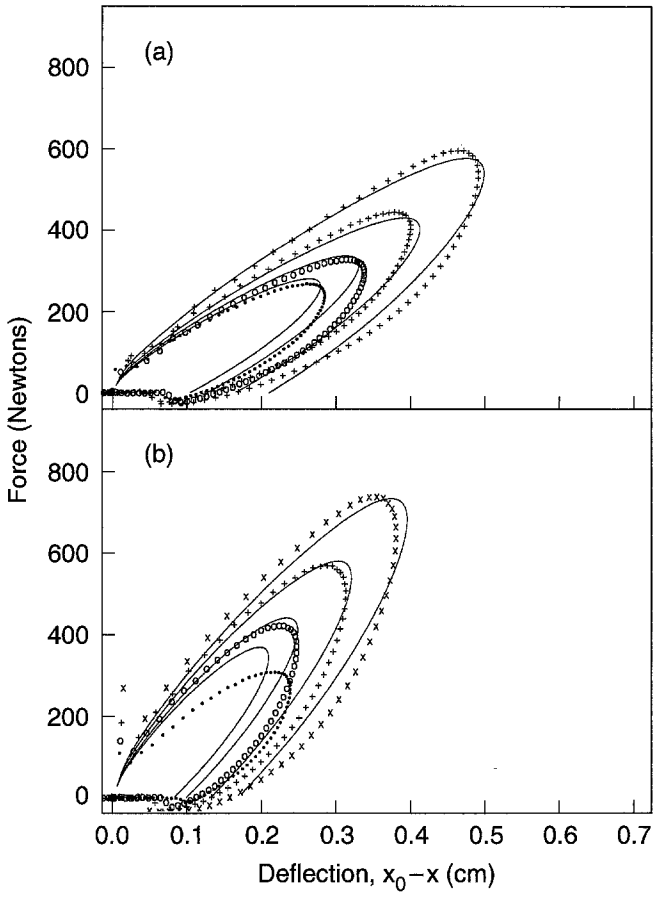


**Fig. 13** a) The same as Fig. 12, except the lines are the theory with an effective area 1.5 times that of the tup. b) The same as in a), except the pad is a square one, 15.24 by 15.24 cm, 2.59 cm thick, the impact velocities are 1.03, 1.23, 1.62, and 2.02 m/s, and the lines are the theory with an effective area 2.4 times that of the tup. $T = 20 \pm 1$ °C

deflection curves for a 2.54 cm diameter tup of mass 1.79 kg, dropped onto a 3.78 cm pad of thickness 2.69 cm at velocities ranging from 1.02 to 1.98 m/s. The predicted curves in Fig. 12 were computed by assuming a constant impact area, A, equal to the impact surface area of the tup. For all drop velocities, the measured forces are much greater than predicted. Presumably, the experimental forces are larger than predicted because of contributions to the force from material elements that are not under the tup, but nevertheless suffer deformation due to the rubber that is forced out from under the tup during the deformation (see Fig. 1 b).

As an empirical correction for this effect, let us suppose that the area of impact in Eq. (3) is a constant "effective area" that includes some of the pad not under the tup. By adjusting this "effective" impact area, we find that a satisfactory fit to the data is achieved when the effective area is 1.5 times that of the tup (see Fig. 13 a). We expect that this "effective impact area" will increase as the area of the pad increases, presumably reaching some saturation value when the pad area becomes much larger than that of the tup. Indeed, Fig. 13 b shows that for the 15.24×15.24 cm square pad, the "effective area" is about 2.4 times that of the tup. By doing drops with a 2.54 cm tup on circular pads of diameter 3.78, 5.03, and 6.27 cm, as well as on a 15.24×15.24 cm square pad, we find that the "effective area" required to obtain a fit increases with pad area, but the rate of increase slows as the pad area becomes much larger than that of the tup. Figure 14 shows the fit obtained for these four pads, all at an impact velocity of around 2.0 m/s. The "effective area" divided by the tup area increases from 1.5 for the 3.78 cm diameter pad, to 2.0 for both the 5.03 and 6.27 cm diameter pads, to 2.4 for the 15.24 cm square sheet.

## Varying shock absorbing material

We have performed similar tests and analyses for another shock-absorbing material, namely Wingfoot XL, a polynorbornene-based material manufactured by a subsidiary of Goodyear. Although Wingfoot XL has viscoelastic characteristics that are significantly different from those of Sorbothane, the agreement between theory and experiment at three different temperatures was at least as good for Wingfoot XL as it is for Sorbothane, even for pads as thin as 1/4 inch (0.63 cm) thick. Thus, we believe that our model is a general one that will successfully predict impact forces for most rubbery materials.

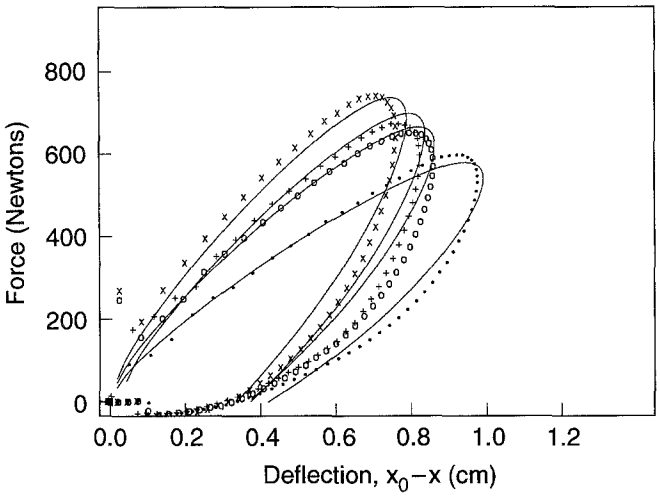


**Fig. 14** The same as Fig. 13, except the pad diameter is varying: 3.78 (●), 5.03 (○), 6.27 (+), and 15.24 (×) cm. The corresponding thicknesses are respectively 2.69, 2.59, 2.46, and 2.59 cm. The impact velocities are, respectively, 1.98, 2.0, 1.99, and 2.02 m/s. The simulations use effective pad areas that are, respectively, 1.5, 2.0, 2.0, and 2.4 times the tup area

## Cushioning efficiency: the *J* curves

The concept of using cushioning efficiency curves, called "*J* curves", for facilitating the design of rubber layers for impact absorption, has been promoted widely by material supplying companies (see Fig. 15). In the trade literature, the "*J* curve" is often taken to be a unique, universal representation of a material's peak force response to various impact parameters mentioned in the previous section. It plots non-dimensional cushioning "efficiency" "*J*" against drop parameters lumped into a single quantity called the impact energy density "*U*", defined as:

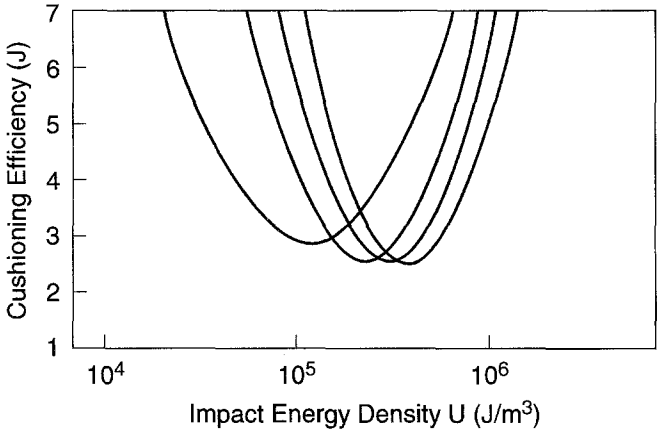


**Fig. 15** Typical "*J* Curves" for different shock absorbing rubbers, where $J \equiv F_{max} x_0 / Wh$ is the dimensionless peak force and $U$ is the impact energy density, $U \equiv Wh/x_0 A_0$ (see E. A. R. Speciality Composites, Engineering Bulletins, Indianapolis, IN, 1993)

$$U \equiv \frac{Wh}{x_0 A_0} \; ; \quad J \equiv \frac{F_{max} x_0}{Wh} \; , \tag{10}$$

where "$W$" (= mg) is the weight of the falling object, $F_{max}$ is the maximum force generated during impact, and $h$ is the drop height, which is related to the impact velocity by $v_0 = \sqrt{2gh}$. Thus despite its name, the so-called "efficiency" $J$ is really the inverse of the cushioning ability of the rubber.

The motivation for plotting data in terms of $U$ and $J$ comes from a dimensional analysis as described in Ref. (10); the equation of motion (3–4) can be rewritten as

$$\frac{x_0^2}{gh} \ddot{X} = \frac{A_0 x_0}{mgh} \frac{1}{X} \sigma\{X(t)\} \; , \tag{11}$$

where $X \equiv x/x_0$ is the dimensionless instantaneous pad thickness, which is related to the instantaneous strain by $\lambda = 1/X$. The stress $\sigma$ is a *functional* of the history of the strain $\lambda(t) = X(t)$; this is denoted by "$X(t)$" in curely brackets. Equation (11) immediately implies that the deformation history $X(t)$, and therefore the peak stress (or peak force), is controlled by two parameters; namely the energy density $U \equiv mgh/A_0 x_0$, and $gh/x_0^2$, which is related to the initial strain rate $v_0/x_0$ by $gh/x_0^2 = 0.5(v_0/x_0)^2$. If the material were purely elastic, then the initial strain rate $v_0/x_0$ would play no role and $J$ would be a function of the impact energy density $U$ only. For real materials, however, the time dependence of the deformation affects the stress, and $J$ should be a function of both $U$ and $v_0/x_0$.

The theoretical minimum value of $J = 1$ corresponds to an ideal impact absorbing material that produces a constant force throughout the entire deflection, and additionally, the dropping mass is brought to rest over a distance equal to the entire thickness $x_0$ of the pad. Thus $J = 1$ corresponds to the theoretical minimum possible peak force during impact.

Figure 16 shows plots of $J$ versus $U$ obtained experimentally and theoretically for Sorbothane 70 by varying the drop velocity at fixed small drop mass, and by varying the drop mass at fixed small drop velocity. At the low and modest impact energies, theory and experiment agree well with each other. For high impact energy densities, although the theory does not agree quantitatively with the experiments (for reasons explored earlier), both curves show minima in $J$ as functions of $U$. At small values of $U$, $J$ is high because for small impact energies, the forces generated by even a small pad deflection are high enough to quickly stop the object's fall; hence most of the pad's thickness is wasted. For high impact energies, the force generated by the deflecting pad is at first insufficient to break the fall, and a high force must be generated when the pad becomes very thin. Thus, the most efficient

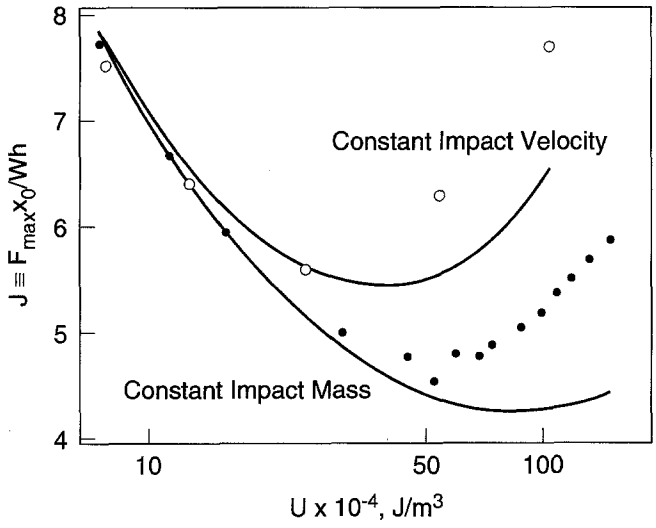


**Fig. 16** The "$J$ Curves", $J \equiv F_{max} x_0 / Wh$, $U \equiv Wh/x_0 A_0$, for a sample of Sorbothane 70, with initial diameter $D_0 = 2.49$ cm, and thickness $x_0 = 2.54$ cm, impacted by a tup of diameter 3.81 cm. The symbols (●) are for a tup mass 1.81 kg, impacted at various velocities. The symbols (○) are for an impact velocity of around 1.1 m/s, with various tup masses. The lines are the theoretical predictions

use of the pad's thickness (and the smallest value of $J$) is obtained for an intermediate impact energy density.

Note that the $J$ curve for a fixed velocity and variable mass is not the same as that for a fixed mass and variable velocity except at the lowest impact energy, where the mass and impact velocities were about the same for both curves. This disagreement is to be expected; on the curve with varying impact velocity $v_0$, the two parameters $U$ and $v_0/x_0$ are varying simultaneously, while on the curve with varying mass, only $U$ is varying.

## Conclusions

We have shown that a classical Hookean viscoelastic constitutive law, combined with measured linear viscoelastic properties, can predict the impact forces and deflections measured with a commercial drop tester when a mass or "tup" with a flat impacting surface is dropped onto a flat pad of commercial impact-absorbing rubber. Good agreement between measured and predicted forces and deflections were obtained for a series of various drop heights, tup masses, impact areas, and pad thicknesses, as long as the deflection of the pad relative to its thickness was small or modest (<50% or so), and as long as the area of the pad was less than or equal to that of the tup. When the pad area is greater than the tup, forces are higher than predicted, but an empirical factor can be introduced to account for the nonuniaxial stretching of the ring of material that extends outside of the impact area. These results show that the material characteristic most relevant to impact absorption is just the ordinary linear viscoelastic relaxation spectrum, which is both simple to measure and widely available from the literature and from manufacturers.

## References

Chen CP, Lakes RS (1990) Design of viscoelastic impact absorbers: optimal material properties. International Journal of Solids & Structures, 26(12):1313–1328

Ferry JD (1980) Viscoelastic Properties of Polymers, 3rd ed., John Wiley & Sons, New York

Freakley PK, Payne AR (1978) Theory and practice of engineering with rubber, Chaptetr 4. Applied Science Publishers Ltd, London

Gent AN, Lindley PB (1959) Internal rupture of bonded rubber cylinders in tension. Proc Royal Soc A 26:195–205

Green MS, Tobolsky AV (1946) A new approach to the theory of relaxing polymeric media. J Chem Phys 14:80

Lindsey GH, Schapery RA, Williams ML, Zak AR (1963) The triaxial tension failure of viscoelastic materials. Aerospace Research Laboratories Office of Aerospace Research, United States Air Force, ARL, pp 63–152, September 1963

Lodge AS (1968) Constitutive equations from molecular network theories for polymer solutions. Rheol Acta 7: 379–392

Meissner J, Stephenson SE, Demarmels A, Portmann P (1982) Multiaxial elongational flows of polymer melts – classification and experimental realization. J Non-Newt Fluid Mech 11:221–237

Treloar LRG (1975) The Physics of Rubber Elasticity, 3rd Ed. Clarendon Press, Oxford

Woolann WE (1968) A study of the dynamics of low energy cushioning materials using scale models. J Cellular Plastics 4:79–83